

Efficient hydroxylation of aromatic compounds catalyzed by an iron(II) complex with H₂O₂

Xiao Wang^a, Tianyong Zhang^a, Bin Li^{a*}, Qiusheng Yang^b and Shuang Jiang^a



A mononuclear iron(II) complex, Et₄N[Fe(C₁₀H₆NO₂)₃], coordinated by three 1-nitroso-2-naphtholate ligands in a fac-N₃O₃ geometry, was initiated to catalyze the direct hydroxylation of aromatic compounds to phenols in the presence of H₂O₂ under mild conditions. Various reaction parameters, including the catalyst dosage, temperature, mole ratio of H₂O₂ to benzene, reaction time and solvents which could affect the hydroxylation activity of the catalyst, were investigated systematically for benzene hydroxylation to obtain ideal benzene conversion and high phenol distribution. Under the optimum conditions, the benzene conversion was 10.2% and only phenol was detected. The catalyst was also found to be active towards hydroxylation of other aromatic compounds with high substrate conversions. The hydroxyl radical formed due to the reaction of the catalyst and H₂O₂ was determined to be the crucial active intermediate in the hydroxylation. A rational pathway for the formation of the hydroxyl radical was proposed and justified by the density functional theory calculations. Copyright © 2014 John Wiley & Sons, Ltd.

Additional supporting information may be found in the online version of this article at the publisher's web-site.

Keywords: iron complex; hydroxylation; H₂O₂; hydroxyl radical

Introduction

Phenols are important organic chemical raw materials that have been produced by multistep reactions with high power consumption for several decades. Recently, the one-step catalytic synthesis of phenols^[1–5] has attracted considerable interest in terms of atom efficiency and environmental friendliness. The key technique for the direct synthesis of phenols lies in the design and synthesis of efficient catalysts. Although it is difficult to recycle and separate compared with heterogeneous catalysts, homogeneous catalysts usually have higher catalytic hydroxylation efficiency.

Iron-based catalyst has been an active research area for many years,^[6–9] as the geologically abundant and non-toxic iron element performs a number of chemically challenging oxidative processes with high precision and reaction rates.^[10–12] Among various iron-based catalysts, iron complexes have been accepted as effective homogeneous catalysts^[13,14] for direct hydroxylation of aromatics. In the hydroxylation of aromatic compounds in the liquid phase, O₂^[15,16] and H₂O₂^[17–19] are usually used as the oxidants. The hydroxylation of aromatic compounds with H₂O₂ is very attractive from the viewpoint of industrial technology and synthetic organic chemistry since H₂O₂ is cheap, environmentally clean and easy to handle. The direct hydroxylation processes oxidized by O₂ generally need to employ severe operating conditions because of the inactive triplet nature of O₂. Understanding the reaction mechanism between the catalysts and the oxidants is still controversial but is of great significance for designing more efficient catalysts.^[20–23]

C.I. Pigment Green 8 (Na[Fe(C₁₀H₆NO₂)₃], PG8) is an iron(II) complex widely used as a cheap organic pigment with excellent color performance,^[24] which was recently adopted as an efficient photocatalyst for selective oxidation of phenol in our group.^[25] In the previous study, we found that PG8 was partly dissolved in

acetonitrile and water, which are usually used as solvents in hydroxylation reactions, and this may suppress its catalytic activity as a homogeneous catalyst. Hence, in this study, the sodium ion in PG8 was replaced by the tetraethylammonium ion, producing soluble Et₄N[Fe(C₁₀H₆NO₂)₃] (PGN) to enhance catalytic activity. PGN was characterized as an iron complex coordinated by three 1-nitroso-2-naphtholate ligands through nitrogen and oxygen atoms. In the presence of H₂O₂, PGN (Fig. 1) was used as an efficient catalyst for the direct hydroxylation of aromatic compounds, as iron complexes containing nitrogen and phenolic oxygen donor atoms have been widely used as efficient catalysts for hydroxylation of various substrates.^[26–28] The hydroxylation proved to proceed with the participation of the hydroxyl radical, as supported by density functional theory (DFT) calculations.

Experimental

Materials and Methods

The chemicals were of analytical grade and used as received. FT-IR spectra were recorded on a Thermo Nicolet 380 spectrophotometer

* Correspondence to: Bin Li, Collaborative Innovation Center of Chemical Science and Engineering (Tianjin), Tianjin Key Laboratory of Applied Catalysis Science and Technology, School of Chemical Engineering and Technology, Tianjin University, Tianjin 300072, People's Republic of China. E-mail: libin@tju.edu.cn

a Collaborative Innovation Center of Chemical Science and Engineering (Tianjin), Tianjin Key Laboratory of Applied Catalysis Science and Technology, School of Chemical Engineering and Technology, Tianjin University, Tianjin 300072, People's Republic of China

b School of Chemical Engineering and Technology, Hebei University of Technology, Tianjin 300130, People's Republic of China

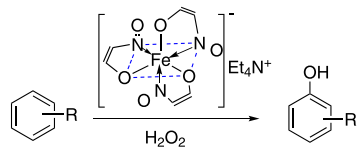


Figure 1. Hydroxylation of aromatic compounds catalyzed by PGN (the —C=C— double bonds stand for the naphthalene ring).

as a KBr pellet. UV–visible absorption spectra were taken on a Thermo Scientific Evolution 300 UV–visible spectrophotometer. TGA was performed using a TA SDT-Q600 apparatus and carried out at dynamic temperature ramp at $10^{\circ}\text{C min}^{-1}$ from ambient temperature to 800°C under nitrogen atmosphere. ^1H NMR and ^{13}C NMR spectra were recorded on a Bruker Avance III 400M spectrometer using tetramethylsilane (TMS) as internal standard in DMSO-d_6 . Elemental analysis was carried out on a Heraeus CHN-O-Rapid fully automatic elemental analyzer with thermal conductivity detection (TMT CHN-O, Bestell-NR 2215001). Electrochemical measurements were carried out in acetonitrile solution ($10^{-4}\text{ mol L}^{-1}$) on a CHI660B (Shanghai Chenhua Instruments) electrochemical workstation using a three-electrode cell. The glassy carbon (0.071 cm^2) working electrode was polished with polishing α -alumina suspension and rinsed with acetonitrile before use. The counter-electrode was a platinum wire. All potentials were recorded with respect to an Ag/Ag^+ reference electrode (0.01 M AgNO_3 and $0.1\text{ M n-Bu}_4\text{NClO}_4$ in acetonitrile) and converted to values versus the ferrocene/ferrocenium redox couple (Fc^+/Fc). X-ray diffraction intensities were collected on a Rigaku MM-007 (rotating anode) diffractometer equipped with a Saturn 70CCD. Data were collected at 113 K using a confocal monochromator with $\text{Mo-K}\alpha$ radiation ($\lambda = 0.71073\text{ \AA}$) in the ω - ϕ scanning mode. Data collection, reduction and absorption correction were performed with the Crystalclear program.^[29] The structure was solved by direct methods and refined with the full-matrix least-squares technique using SHELXS-97 and SHELXL-97^[30] programs, respectively. Hydrogen atoms were included in their calculated positions. Some unresolved solvent present in the structure of PGN was found to be highly disordered, so the SQUEEZE procedure of the PLATON program^[31] was used, suggesting 32 electrons in one unit cell. The molecular structure diagram (Fig. 4) was created with the SHELXTL program.^[32] The quantitative and qualitative analysis of the aromatics and phenols were carried out with an Agilent 6890 N gas chromatograph equipped with capillary column ($30\text{ m} \times 0.25\text{ mm} \times 0.25\text{ }\mu\text{m}$) and flame ionization detector. Density functional theory calculations were carried out at B3LYP/6-31G+d level implemented with the Gaussian 09 program.^[33]

Preparation of PGN

PG8 was synthesized according to the literature (yield 98.0%).^[25] Tetraethylammonium chloride (166 mg, 1.0 mmol) was added to a *N,N*-dimethylformamide solution (40.0 ml) of PG8 (595 mg, 1.0 mmol) and the mixture was stirred for 2 h at room temperature. After the addition of diethyl ether (100 ml) to the solution, PGN precipitated out and was collected as a dark-green solid (630 mg, 89.7%). Anal. Calcd for PGN ($\text{C}_{38}\text{H}_{38}\text{FeN}_4\text{O}_6$): C, 64.96; H, 5.41; N, 7.98. Found: C, 64.73; H, 5.54; N, 7.75%. UV–visible λ_{max} (acetonitrile) (nm): 345, 430, 690 (ϵ ($\text{dm}^3\text{ mol}^{-1}\text{ cm}^{-1}$)) 37 200, 24 800, 32 400). FT-IR (KBr) ν_{max} (cm^{-1}): 1593 (C=C phenyl),

1512 (Ar–C–O), 1453 (Ar–N=O), 1360 (=C–H phenyl). ^1H NMR (400 MHz, DMSO-d_6) see Fig. S1, supporting information), δ 8.87 (d, $J = 8.3\text{ Hz}$, 3H, C9–H), 7.90 (d, $J = 9.3\text{ Hz}$, 3H, C4–H), 7.76 (d, $J = 7.9\text{ Hz}$, 3H, C6–H), 7.51 (dd, $J = 7.4\text{ Hz}$, 3H, C8–H), 7.31 (dd, $J = 7.9\text{ Hz}$, 7.4 Hz, 3H, C7–H), 7.12 (d, $J = 9.3\text{ Hz}$, 3H, C3–H), 3.20 (q, $J = 7.0\text{ Hz}$, 8H, C11–H), 1.16 (t, $J = 7.0\text{ Hz}$, 12H, C12–H). ^{13}C NMR (100 MHz, DMSO-d_6) see Fig. S1), δ 183.6 (C2), 151.4 (C1), 137.5 (C4), 130.6 (C5), 127.7 (C6), 125.3 (C10), 124.3 (C8, C9), 123.2 (C7), 121.4 (C3), 51.4 (C11), 7.04 (C12).

Hydroxylation of Aromatic Compounds

Hydroxylation of the aromatic compounds with H_2O_2 (30% in water) was carried out in a 50 ml round-bottom flask equipped with a reflux condenser and a magnetic stirrer. In a typical reaction, PGN was dissolved in 20.0 ml acetonitrile. After the solution was heated to the desired temperature, the aromatic substrates were added. A certain amount of H_2O_2 was added to initiate the hydroxylation. All the experiments were conducted under ambient conditions. After stirring for several hours, a small amount of the mixture was centrifuged and analyzed by gas chromatography.

Results and Discussion

Thermal Stability of PGN

Thermal stability of PGN was checked by TG analysis and the derivative thermogravimetry (DTG) curve is shown in Fig. 2. A rapid weight loss originated from the decomposition of the ligands from 280 to 300°C was observed. A slower weight loss resulting from the volatilization of the early decomposition products of PGN occurred from 600 to 800°C . We concluded from the results of the TG and DTG analysis that PGN showed great heat resistance.

Electrochemical Measurements of PGN

The cyclic voltammogram (CV) of PGN showed a reversible redox couple and the oxidation event which assigned to $\text{Fe}^{2+}/\text{Fe}^{3+}$ was at a low potential of 0.017 V (vs. Fc^+/Fc) as illustrated in Fig. 3. The low oxidation potential implied the strong electron donating ability of the 1-nitroso-2-naphtholate ligands to the iron center, which also suggested that PGN could be oxidized easily to the iron(III) species under appropriate conditions.

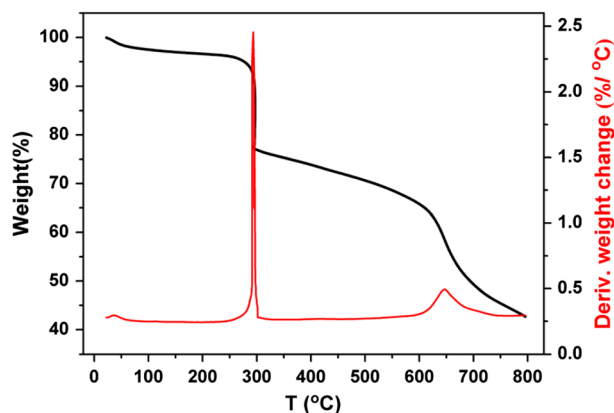


Figure 2. The TG and DTG analysis of PGN.

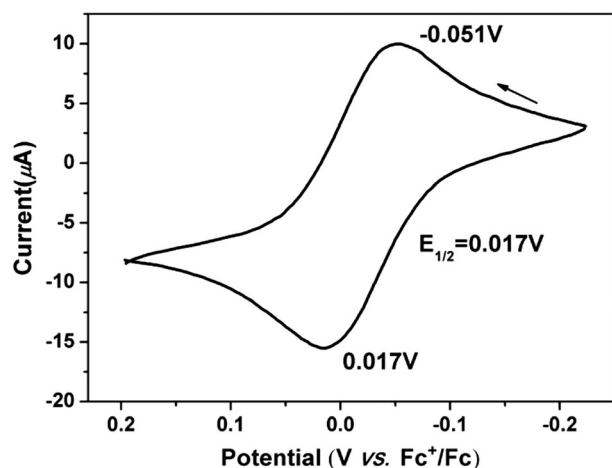


Figure 3. Cyclic voltammogram of PGN in de-aerated acetonitrile containing 0.1 M *n*-Bu₄NClO₄ at 25°C, scan rate 0.05 V s⁻¹.

X-Ray Crystal Structure Determination

In the literature, structures of metal complexes coordinated by the 1-nitroso-2-naphtholate ligand feature coordination geometries based on six oxygen atoms^[34,35] or three nitrogen atoms and three oxygen atoms.^[36,37] In order to obtain the exact structure of PGN, an X-ray crystal structure determination was carried out. Single crystals suitable for X-ray crystallographic analysis were obtained by slow diffusion of *n*-hexane into the dichloromethane solution of PGN. Details of the crystallographic data are summarized in Table 1. CCDC975043 contains the supplementary crystallographic data for this paper. The molecular structure of PGN (Fig. 4) showed a slightly distorted octahedral iron center coordinated by the 1-nitroso-2-naphtholate ligands through nitrogen and oxygen atoms, each forming a five-membered chelate ring. All the three nitrogen atoms occupied

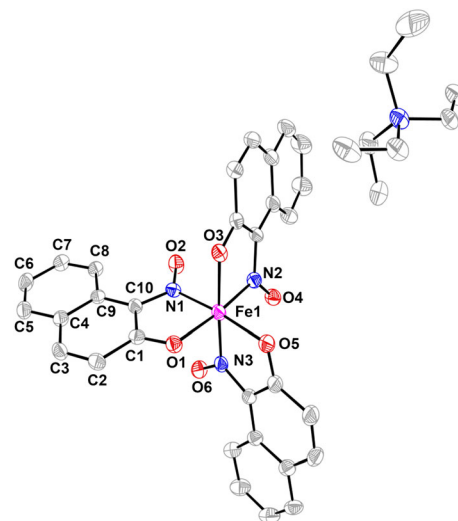


Figure 4. X-ray crystal structure of PGN (ellipsoids at 50% probability level, the hydrogen atoms are omitted for clarity). Selected bonds lengths (Å): Fe1—N1 1.887(2), Fe1—O1 1.9652(16), Fe1—N2 1.854(2), Fe1—O3 1.9635(16), Fe1—O5 1.9636(19), Fe1—N3 1.858(2).

one triangular face, establishing PGN to be the *fac*-isomer; the three coordinated oxygen atoms occupied the *trans* positions to nitrogen on the opposite triangular face.

Hydroxylation of Benzene to Phenol

Hydroxylation of benzene was performed in acetonitrile with H₂O₂ as the oxidant. A blank experiment (Table 2, entry 1) was conducted in which no phenol or dihydroxybenzenes were detected. We also observed that the soluble PGN exhibited higher benzene conversion and phenol distribution than PG8, which was partly dissolved under the same conditions (Table 2, entries 2 and 3). Thus PGN was used as a homogeneous catalyst in this study. Some parameters such as the catalyst dosage, temperature, mole ratio of H₂O₂ to benzene, reaction time and solvents were investigated systematically to obtain ideal benzene conversion and high phenol distribution.

Table 1. Crystallographic data	
Empirical formula	C ₃₈ H ₃₈ FeN ₄ O ₆
Formula weight	702.57
Space group	C2/c
Crystal size (mm)	0.10 × 0.20 × 0.20 mm
Crystal system	Monoclinic
<i>a</i> (Å)	16.827(3)
<i>b</i> (Å)	14.023(3)
<i>c</i> (Å)	28.417(6)
β (°)	91.40(3)
<i>V</i> (Å ³)	6704(2)
<i>Z</i>	8
ρ (g cm ⁻³)	1.392
μ (mm ⁻¹)	0.504
<i>F</i> (000)	2944
θ_{\max} (°)	27.9
No. of measured reflections	31753
No. of unique reflections and <i>R</i> _{int}	7856 and 0.061
No. of observed reflections [<i>I</i> ≥ 2σ(<i>I</i>)]	6064
Goodness-of-fit on <i>F</i> ²	1.10
<i>R</i> , <i>wR2</i> [<i>I</i> ≥ 2σ(<i>I</i>)]	0.058, <i>wR2</i> = 0.132
<i>R</i> , <i>wR2</i> (all data)	0.078, <i>wR2</i> = 0.144

Table 2. Blank experiment and effects of different catalysts ^a					
Entry	Catalyst	Benzene conversion ^b (%)	Product distributions ^c (%)		
			Phenol	CAT ^d	HQ ^e
1	None	0	N.D. ^f	N.D.	N.D.
2	PG8	17.2	52.9	21.4	25.7
3	PGN	25.7	55.2	19.8	25.0

^a60°C; benzene, 1.0 ml; catalyst, 0.14 mmol; acetonitrile, 20.0 ml; reaction time, 3 h; *n*(H₂O₂):*n*(benzene) = 3.
^bMoles of benzene converted based on the products/initial moles of benzene.
^cMoles of phenol (CAT or HQ) produced/moles of all the products detected by GC.
^dCAT, catechol.
^eHQ, hydroquinone.
^fN.D., not detected.

Effects of PGN Dosage

The influence of catalyst dosage on benzene conversion and product distribution are illustrated in Table 3. The benzene conversion increased first, which is initially attributed to more PGN being exposed to react with H_2O_2 , forming more active intermediates to oxidize benzene; conversion then decreased as a result of accelerated non-productive decomposition of H_2O_2 with incremental PGN dosage. Accompanied by the increased benzene conversion, catechol and hydroquinone were detected due to the further oxidation of phenol, which could be concluded from the observed lower phenol distribution when 0.1 g or more PGN was used. Under the condition that more H_2O_2 decomposed on the surface of the catalyst when more than 0.1 g PGN was added, we also found that the phenol distribution slightly increased owing to the reduced amount of H_2O_2 which could be used to oxidize phenol to dihydrobenzenes. Although the phenol distribution was 100% when 0.05 g PGN was added, benzene conversion was low. The highest benzene conversion was obtained when 0.1 g PGN was added. From the economic point of view, 0.1 g catalyst was the appropriate dosage since the phenol distribution was comparable with that obtained when more PGN was used.

Effects of Temperature

The effects of temperature on the hydroxylation of benzene are shown in Fig. 5. With an increase in temperature, benzene conversion increased first and then decreased. Although the phenol distribution was 100% at 30 and 40°C, only a small amount of benzene was converted because a longer induction period under low temperature prevented the formation of phenols. Higher temperature sped up the reaction, which resulted in higher benzene conversion. Decreased phenol distribution was also observed as a result of the accelerated further oxidation of phenol under higher temperature. The relative high benzene conversion (16.6%) and phenol distribution (76.0%) were obtained at 50°C.

Effects of Mole Ratio of H_2O_2 to Benzene

As illustrated in Fig. 6, benzene conversion and product distribution were greatly influenced by the mole ratio of H_2O_2 to benzene. The benzene conversion increased with added increments of H_2O_2 , which was lower than 10% under a lower mole ratio of H_2O_2 to benzene. Dihydroxybenzenes were not detected until the mole ratio of H_2O_2 to benzene reached 2. The phenol distribution decreased and dihydroxybenzene distribution increased

Table 3. Effects of PGN dosage on hydroxylation of benzene^a

Entry	PGN (g)	Benzene conversion (%)	Product distribution (%)		
			Phenol	CAT	HQ
1	0.05	7.5	100	N.D.	N.D.
2	0.1	25.7	55.2	19.8	25.0
3	0.2	21.2	57.4	18.2	24.4
4	0.3	17.6	59.7	17.6	22.7

^a60°C; benzene, 1.0 ml; acetonitrile, 20.0 mL; reaction time, 3 h; $n(\text{H}_2\text{O}_2):n(\text{benzene}) = 3$.

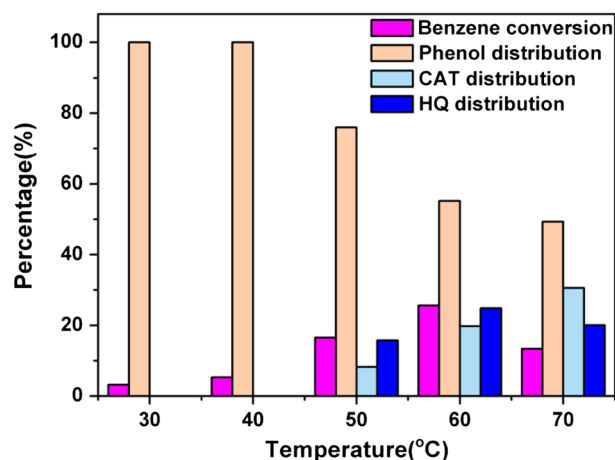


Figure 5. Effects of temperature on hydroxylation of benzene. Benzene, 1.0 ml; PGN, 0.1 g; acetonitrile, 20.0 ml; reaction time, 3 h, $n(\text{H}_2\text{O}_2):n(\text{benzene}) = 3$.

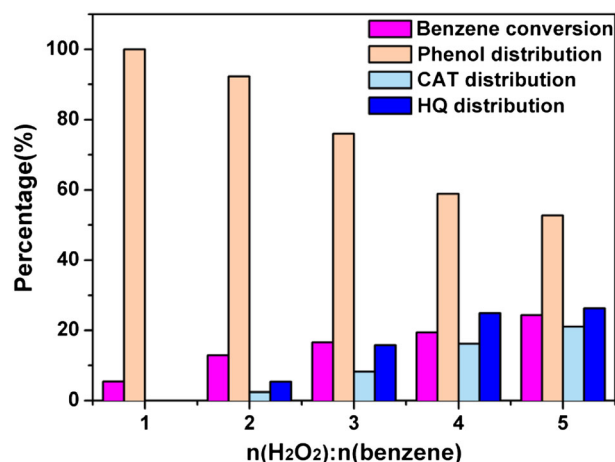


Figure 6. Effects of mole ratio of H_2O_2 to benzene on hydroxylation of benzene. 50°C; benzene, 1.0 ml; PGN, 0.1 g; acetonitrile, 20.0 ml; reaction time, 3 h.

gradually because of the further oxidation of phenol with excess H_2O_2 . When the mole ratio of H_2O_2 to benzene was 2, higher phenol distribution (92.3%) and ideal benzene conversion (12.9%) was observed.

Effects of Reaction Time

Table 4 showed that the higher benzene conversion and lower phenol distribution were achieved over long reaction times. When the mole ratio of H_2O_2 to benzene was 2, only phenol was detected in the first 2 h, which was then oxidized to dihydroxybenzenes after a longer time. As a result of further oxidation, a decreased phenol distribution was obtained. The effects of reaction time on the hydroxylation of benzene to phenol implies that the dihydroxybenzenes were formed only when phenol had accumulated to a certain extent. In the first 3 h, 12.9% benzene was consumed at high reaction rate, which then slowed with reduced reactant concentrations as time elapsed.

Table 4. Effects of reaction time on hydroxylation of benzene^a

Entry	Time (h)	Benzene conversion (%)	Products distributions (%)		
			Phenol	CAT	HQ
1	1	6.8	100	N.D.	N.D.
2	2	10.2	100	N.D.	N.D.
3	3	12.9	92.3	2.4	5.3
4	4	13.3	72.3	10.1	17.6
5	5	14.9	57.2	19.6	23.2

^a50°C; benzene, 1.0 mL; PGN, 0.1 g; acetonitrile, 20.0 mL; $n(\text{H}_2\text{O}_2):n(\text{benzene}) = 2$.

Effects of Solvents

The hydroxylation of benzene to phenol was carried out in different solvents and the results are shown in Table 5. The results showed that the activity of the catalyst was greatly influenced by the solvents. It appears that acetonitrile was the only effective solvent among the studied solvents, although its influence on hydroxylation has not been unambiguously elucidated in this study. In the catalytic hydroxylation system involving an iron-based catalyst and H_2O_2 , the hydroxyl radical is likely to be formed and act as the active intermediate, as reported in the literature.^[38–40] Combining the fact that acetone and ethanol are usually used as hydroxyl radical scavengers^[41] and the results that no phenol was detected in acetone or ethanol, we speculate that the hydroxylation of benzene to phenol catalyzed by PGN proceeded through a hydroxyl radical mechanism.

Effects of Hydroxyl Radical Scavenger

In order to verify our postulate that the hydroxyl radical was formed in the hydroxylation of benzene to phenol in the presence of H_2O_2 , the effects of addition of hydroxyl radical scavenger on the production of phenol were investigated by adding ethanol to the reaction system. Since the hydroxyl radical produced in the hydroxylation will react with both benzene and ethanol, the relationship between the concentration of phenol and that of ethanol can be expressed by the following equation:

$$\frac{[\text{Phenol}]_0}{[\text{Phenol}]} \approx 1 + \frac{k_2[\text{Ethanol}]}{k_1[\text{Benzene}]}$$

where $[\text{Phenol}]_0$ and $[\text{Phenol}]$ represent phenol produced without and with added ethanol; $[\text{Ethanol}]$ and $[\text{Benzene}]$ are initial concentration of ethanol and benzene; and k_1 and k_2 are rate constants of the reactions between benzene or ethanol and the hydroxyl radical.

Table 5. Effects of solvents on hydroxylation of benzene^a

Entry	Solvent	Benzene conversion (%)	Product distribution (%)		
			Phenol	CAT	HQ
1	Acetonitrile	10.2	100	N.D.	N.D.
2	Acetone	—	N.D.	N.D.	N.D.
3	Ethanol	—	N.D.	N.D.	N.D.
5	1,4-Dioxane	—	N.D.	N.D.	N.D.

^a50°C; benzene, 1.0 ml; PGN, 0.1 g; solvents, 20.0 ml; reaction time, 2 h; $n(\text{H}_2\text{O}_2):n(\text{benzene}) = 2$.

As reported in the literature,^[42,43] if the hydroxyl radical is formed in benzene hydroxylation, $[\text{Phenol}]_0/[\text{Phenol}]$ should be linear with $[\text{Ethanol}]$. $[\text{Phenol}]_0/[\text{Phenol}]$ was plotted as a function of $[\text{Ethanol}]$, which was almost linear as shown in Fig. 7; we thus concluded that the hydroxyl radical was formed and acted as the key active species for direct hydroxylation of benzene to phenol.

In the PGN-catalyzed hydroxylation of benzene, under the optimum conditions (1.0 ml benzene, 0.1 g PGN, 50°C, 20.0 ml acetonitrile, mole ratio of H_2O_2 to benzene = 2), benzene conversion was 10.2% and phenol distribution was 100%. Benzene conversion was higher in the hydroxylation catalyzed by similar iron polyazadentate complexes^[14] in the presence of H_2O_2 due to the participation of the highly selective iron-oxo species. In our study, benzene conversion was at a relative low level in which the hydroxyl radical was proved to be the active species. In the catalytic hydroxylation of benzene to phenol with the non-selective and highly active hydroxyl radicals as the active species, the higher conversion of the substrates was usually accompanied by lower selectivity as the hydroxyl radical would react with the hydroxylated product to produce further oxidation products such as dihydroxybenzenes. Thus the benzene conversion should be carefully controlled to obtain high phenol selectivity.

Hydroxylation of Aromatic Compounds

Furthermore, PGN was also able to catalyze the hydroxylation of a series of aromatic compounds to corresponding phenols, which revealed good substrate adaptability. As shown in Table 6, substrates with activating *ortho*-/*para*-directing substituents like toluene, phenol and fluorobenzene were converted to both *ortho*- and *para*-phenols. The nature of the phenols of the hydroxylation of different substrates by PGN suggested that the reaction involved a non-selective species, which was consistent with the conclusion that the hydroxyl radical was formed in the hydroxylation from the previous experiments in this study.

It has been proved that the first step of the reaction between the aromatic compounds and hydroxyl radical involves the electrophilic addition of the hydroxyl radical to the aromatic compound to form cyclohexadienyl radical.^[44,45] Under the same conditions, the hydroxyl radical was prone to attack the electron-rich benzene ring. Consequently, phenol and toluene, which are more prone to react with the hydroxyl

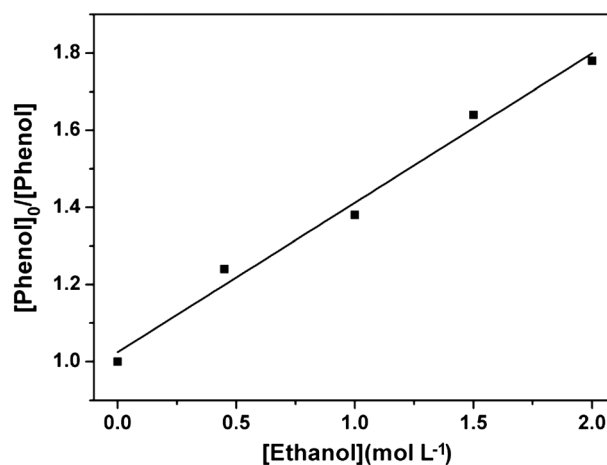
**Figure 7.** Effects of ethanol concentration on formation of phenol.

Table 6. Hydroxylation of different substrates catalyzed by PGN^a

Entry	Substrate	Conversion (%)	Products distributions (%)	
1	Toluene	16.5	<i>o</i> -Cresol 44.2	<i>p</i> -Cresol 55.8
2	Phenol	18.1	Catechol 45.9	Hydroquinone 54.1
3	Naphthalene	11.3	1-Naphthol 100	
4	Fluobenzene	5.4	<i>o</i> -Fluorophenol 42.6	<i>p</i> -Fluorophenol 57.4
5	Benzene	10.2	Phenol 100	

^a50°C; aromatic compounds, 11.3 mmol; PGN, 0.1 g; acetonitrile, 20.0 ml; reaction time, 2 h; $n(\text{H}_2\text{O}_2):n(\text{aromatics}) = 2$.

radical, compared with naphthalene, fluorobenzene and benzene, exhibited higher conversions.

Proposed Mechanism and DFT Calculations

According to the experiments above and the conclusion that the hydroxyl radical was the active species in the direct hydroxylation of the aromatic compounds catalyzed by PGN with H_2O_2 , we proposed a rational catalytic cycle with the participation of PGN involving production of the hydroxyl radical, as illustrated in Fig. 8.

To further examine the deduced pathway for production of the hydroxyl radical, DFT calculations were conducted. The sum of the free energies of PGN (the anion), H_3O^+ and H_2O_2 were taken as zero energy. The optimized structure of PGN (the anion) matched well the geometric data determined by X-ray diffraction, which supported our choice for the function and basis set and thus lent confidence to the correctness of the computation. Optimized structures of PGN (the anion) as well as other intermediates are shown in Figs S2–S8, and selected bond lengths and angles are listed in Tables S1–S7.

The main results of the DFT study are also illustrated by the free energy profile (shown in parentheses in Fig. 8). Since PGN was a hexa-coordinated complex with an iron(II) center, there was no open site for the attack of H_2O_2 molecule to the iron(II) center. The first step should be the protonation of PGN, which caused Fe–O bond cleavage ($\Delta G^\ddagger < < 0 \text{ kJ mol}^{-1}$) between the

low spin iron(II) center of PGN and the oxygen atom of the naphtholate ligand. The low oxidation potential of the $\text{Fe}^{2+}/\text{Fe}^{3+}$ event (0.017 V vs. Fc^+/Fc) illustrated in Fig. 3 also indicated the easy cleavage of the Fe–O bond via protonation due to the strong electron-donating ability of the 1-nitroso-2-naphtholate ligands. The penta-coordinated neutral complex **IM2**^[46] was formed by the configuration inversion with an energy barrier of $17.75 \text{ kJ mol}^{-1}$, which provided an available open site for the coordination of H_2O_2 to the iron(II) center. The homolysis of the O–O bond of the H–O–O–H cluster attached to the iron center in **IM3** then caused the production of a hydroxyl radical and **IM4**, followed by oxidation of the ferrous iron to the ferric in **IM4** ($\Delta G^\ddagger = -15.08 \text{ kJ mol}^{-1}$), which also could be concluded from the low oxidation potential of the $\text{Fe}^{2+}/\text{Fe}^{3+}$ couple. Here, the theoretical calculations in conjunction with the electrochemistry results demonstrated a reasonable pathway of oxidizing PGN to **IM4**. On the basis of the above analysis, we draw a conclusion that the proposed production pathway of the hydroxyl radical was thermodynamically rational.

The aromatics were attacked readily by the highly active hydroxyl radical to form the cyclohexadienyl radical, which could then react with **IM4** to produce phenol. Simultaneously, **IM5** with an iron(II) center was formed from **IM4** via accepting one electron from the cyclohexadienyl radical inferred from the literature.^[47,48] This needs further verification because the reaction process and the calculations including the active radicals were complicated. The nucleophilic intermediate **IM5** was protonated easily to produce **IM6**, in which the water molecule could be released to form **IM2** with an energy barrier of $10.36 \text{ kJ mol}^{-1}$ to fulfill the catalytic cycle.

Conclusions

In this study, PGN was explored for catalytic potential. The mononuclear iron complex PGN was coordinated by the 1-nitroso-2-naphtholate ligands, which define a fac- N_3O_3 donor set. Under the conditions that 1.0 ml benzene, 0.1 g PGN, 50°C, 20.0 ml acetonitrile as the solvent, the mole ratio of H_2O_2 to benzene was 2, benzene conversion was 10.2% and phenol distribution was 100%. Under the same conditions, PGN was also able to catalyze the hydroxylation of other aromatic compounds to the corresponding phenols with high substrate conversion. The hydroxyl radical mechanism was proved to dominate the hydroxylation. A rational pathway for the formation of the hydroxyl radical was proposed in which PGN was oxidized to an iron(III) species accompanied by the release of a hydroxyl radical justified by the theoretical results. Given the reactivity and broad substrate scope demonstrated, we anticipate that this study reveals a new way for the direct hydroxylation of aromatic compounds. Based on the activity of PGN, we deduce

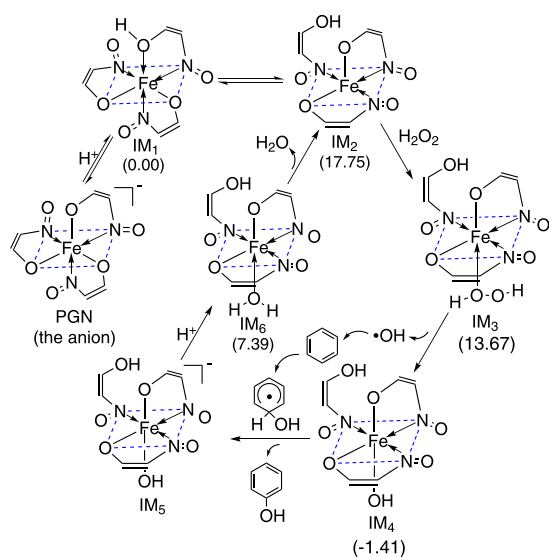


Figure 8. Proposed catalytic cycle (the naphthalene ring is omitted as the —C=C— double bond). The Gibbs free energy profiles (kJ mol^{-1}) of the intermediates are shown in parentheses.

that the 1-nitroso-2-naphtholate ligand, which offers both nitrogen and oxygen atoms as the coordination atoms, shows promise for the design of efficient iron complexes for the hydroxylation of aromatic compounds.

Acknowledgments

This work was supported by the National Natural Science Foundation of China (Nos. 21103121, 21276187, 21236001) and Tianjin Municipal Natural Science Foundation (13JCQNJC05800).

References

- [1] P. Borah, X. Ma, K. T. Nguyen, Y. Zhao, *Angew. Chem. Int. Ed.* **2012**, *51*, 7756.
- [2] T. Jiang, W. Wang, B. Han, *New J. Chem.* **2013**, *37*, 1654.
- [3] P. Zhao, Y. Leng, J. Wang, *Chem. Eng. J.* **2012**, *204–206*, 72.
- [4] B. Lee, H. Naito, T. Hibino, *Angew. Chem. Int. Ed.* **2012**, *51*, 440.
- [5] O. V. Makhlynets, E. V. Rybak-Akimova, *Chem.-Eur. J.* **2010**, *16*, 13995.
- [6] O. Shoji, T. Kunimatsu, N. Kawakami, Y. Watanabe, *Angew. Chem. Int. Ed.* **2013**, *52*, 6606.
- [7] Y. Wang, Z. Fu, X. Wen, C. Rong, W. Wu, C. Zhang, J. Deng, B. Dai, S. R. Kirk, D. Yin, *J. Mol. Catal. A: Chem.* **2014**, *383–384*, 46.
- [8] X. Zhao, Z. Sun, Z. Zhu, A. Li, G. Li, X. Wang, *Catal. Lett.* **2013**, *143*, 657.
- [9] S. Yang, G. Liang, A. Gu, H. Mao, *Ind. Eng. Chem. Res.* **2012**, *51*, 15593.
- [10] C. L. Sun, B. J. Li, Z. J. Shi, *Chem. Rev.* **2011**, *111*, 1293.
- [11] C. Bolm, J. Legtos, J. L. Pailh, L. Zani, *Chem. Rev.* **2004**, *104*, 6217.
- [12] C. Walling, R. A. Johnson, *J. Am. Chem. Soc.* **1975**, *97*, 363.
- [13] A. Thibon, V. Jollet, C. Ribal, K. Senechal-David, L. Billon, A. B. Sorokin, F. Banse, *Chem.-Eur. J.* **2012**, *18*, 2715.
- [14] A. Thibon, J.-F. Bartoli, R. Guillot, J. Sainon, M. Martinho, D. Mansuy, F. Banse, *J. Mol. Catal. A: Chem.* **2008**, *287*, 115.
- [15] M. Tada, R. Bal, T. Sasaki, Y. Uemura, Y. Inada, S. Tanaka, M. Nomura, Y. Iwasawa, *J. Phys. Chem. C* **2007**, *111*, 10095.
- [16] A. Dennig, N. Lültsdorf, H. Liu, U. Schwaneberg, *Angew. Chem. Int. Ed.* **2013**, *52*, 8459.
- [17] A. N. Kharat, S. Moosavikia, B. T. Jahromi, A. Badiei, *J. Mol. Catal. A: Chem.* **2011**, *348*, 14.
- [18] D. Bianchi, L. Balducci, R. Bortolo, R. D'Aloisio, M. Ricci, G. Spanò, R. Tassinari, C. Tonini, R. Ungarelli, *Adv. Synth. Catal.* **2007**, *349*, 979.
- [19] C. K. Modi, P. M. Trivedi, *Adv. Mater. Lett.* **2012**, *3*, 149.
- [20] J. L. Li, X. Zhang, X. R. Huang, *Phys. Chem. Chem. Phys.* **2012**, *14*, 246.
- [21] S. P. de Visser, K. Oh, A.-R. Han, W. Nam, *Inorg. Chem.* **2007**, *46*, 4632.
- [22] T. Kurata, Y. Watanabe, M. Katoh, Y. Sawaki, *J. Am. Chem. Soc.* **1988**, *110*, 7472.
- [23] D. T. Sawyer, C. Kang, A. Llobet, C. Redman, *J. Am. Chem. Soc.* **1993**, *115*, 5817.
- [24] BASF, DE Patent 356973C, **1922**.
- [25] H. Shi, T. Zhang, T. An, B. Li, X. Wang, *Curr. Org. Chem.* **2012**, *16*, 3002.
- [26] L. Chen, Y. Xiang, T. Feng, *Appl. Organomet. Chem.* **2012**, *26*, 108.
- [27] E. A. Karakhanov, A. L. Maximov, Y. S. Kardasheva, V. A. Skorkin, S. V. Kardashev, E. A. Ivanova, E. Lurie-Luke, J. A. Seeley, S. L. Cron, *Ind. Eng. Chem. Res.* **2010**, *49*, 4607.
- [28] S. Tanase, J. Reedijk, R. Hage, G. Rothenberg, *Top. Catal.* **2010**, *53*, 1039.
- [29] CrystalStructure 3.7.0 and Crystalclear 1.36: Crystal Structure Analysis Package, Rigaku and Rigaku/MSC, TX, **2000–2005**.
- [30] G. M. Sheldrick, *Acta Crystallogr.* **2008**, *A64*, 112.
- [31] P. van der Sluis, A. L. Spek, *Acta Crystallogr.* **1990**, *A46*, 194.
- [32] Bruker Advanced X-ray Solutions SHELXTL (version 6.10), Bruker AXS Inc., Madison, WI, **2000**.
- [33] M. J. Frisch, G. W. Trucks, H. B. Schlegel, *et al.*, Gaussian 09 (Revision D01), Gaussian, Inc., Wallingford, CT, **2010**.
- [34] J. Charalambous, M. J. Frazer, R. Sims, *Inorg. Chim. Acta* **1976**, *18*, 247.
- [35] D. Malcolm, P. J. Broadbent, US Patent 2009212554A1, **2009**.
- [36] E. I. Aksiment'eva, V. P. D'yakonov, Z. A. Samoilenko, V. V. Shapovalov, S. N. Pekhota, *Russ. J. Gen. Chem.* **2000**, *70*, 1581.
- [37] P. Basu, S. Pal, A. Chakravorty, *J. Chem. Soc. Chem. Commun.* **1989**, *15*, 977.
- [38] G. Tanarungsun, W. Kiatkittipong, S. Assabumrungrat, H. Yamada, T. Tagawa, P. Praserttham, *J. Ind. Eng. Chem.* **2007**, *13*, 444.
- [39] X. Hu, L. Zhu, X. Wang, B. Guo, J. Xu, G. Li, C. Hu, *J. Mol. Catal. A: Chem.* **2011**, *342–343*, 41.
- [40] K. M. Parida, S. Singha, P. C. Sahoo, *Catal. Lett.* **2010**, *136*, 155.
- [41] J. Okamura, S. Nishiyama, S. Tsuruya, M. Masai, *J. Mol. Catal. A: Chem.* **1998**, *135*, 133.
- [42] Y. Y. Gu, X. H. Zhao, G. R. Zhang, H. M. Ding, Y. K. Shan, *Appl. Catal. A: Gen.* **2007**, *328*, 150.
- [43] Y.-k. Masumoto, R. Hamada, K. Yokota, S. Nishiyama, S. Tsuruya, *J. Mol. Catal. A: Chem.* **2002**, *184*, 215.
- [44] A. Kunai, S. Hata, S. Ito, K. Sasaki, *J. Am. Chem. Soc.* **1986**, *108*, 6012.
- [45] S. Ito, A. Mitarai, K. Hikino, M. Hiram, K. Sasaki, *J. Org. Chem.* **1992**, *57*, 6937.
- [46] M. S. Masoud, T. M. Salem, M. M. Elessawy, *Syn. React. Inorg. Met.* **1983**, *13*, 79.
- [47] D. I. Metelitsa, *Russ. Chem. Rev.* **1971**, *40*, 563.
- [48] G. V. Buxton, J. R. Langan, J. R. L. Smith, *J. Phys. Chem.* **1986**, *90*, 6309.

Supporting Information

Additional supporting information may be found in the online version of this article at the publisher's web-site.